

Research papers

Evaluation of parametric precipitation models in reproducing tropical cyclone rainfall patterns



John T. Brackins, Alfred J. Kalyanapu*

Department of Civil and Environmental Engineering, Tennessee Technological University, Cookeville, TN, USA

ARTICLE INFO

This manuscript was handled by A. Bardossy, Editor-in-Chief, with the assistance of Roger Moussa, Associate Editor

Keywords:

Tropical cyclones
Rainfall
Flood risk
Joint flooding

ABSTRACT

Current flood mapping practices in the United States model both storm surge and riverine flooding in coastal regions. In regions where the hazards overlap, independence and non-concurrence are generally assumed, although recent literature has noted several cases of tropical cyclones (TCs) where storm surge and rainfall-runoff interacted nonlinearly, violating this assumption. In order to evaluate the effects of the nonlinear interactions on flood risk statistics using traditional methods, i.e. by using simulation suites of physically-based flood hazard models with varied TC characteristics, it is necessary to couple the rainfall-runoff and storm surge components into a single simulation framework. In order to accomplish this efficiently, use of a parametric TC rainfall model is proposed. Four such models were obtained by the authors: R-CLIPER (Rainfall Climatology and Persistence), IPET (Interagency Performance Evaluation Task Force Rainfall Analysis), PHRaM (Parametric Hurricane Rainfall Model), and P-CLIPER (PDF Precipitation-Climatology and Persistence). The objective of the current study is to compare precipitation fields produced by four existing parametric TC rainfall models and then to select the most appropriate model for inclusion in future combined flooding studies. Meteorological skill metrics were used to evaluate rainfall models for 67 Atlantic TCs affecting the United States from 2004 through 2017. Of the four models evaluated, the highly simplified IPET rainfall model demonstrated the most skill at reproducing storm-total precipitation for thresholds above 75 mm (3 in.); however, the skill metrics obtained indicate that none of the models is suitable for direct use in combined flooding studies at this time.

1. Introduction

While US coastal watershed counties account for less than 20% of the land area, 52% of the US population resides in these counties (Crossett et al. 2013). Tropical cyclones (TCs) are a major contributor to the flood threat in coastal watershed counties, through a variety of mechanisms: (1) rainfall-runoff flooding from TC rainfall, (2) coastal flooding (including effects of storm surge, wave setup, breaking waves, and tides), or (3) interactions between rainfall-runoff and coastal effects. Mechanism (1) was largely to blame for inundation of Harris County and Houston, Texas, during 2017 Hurricane Harvey, as the storm produced over 1524 mm (60 in.) of rainfall within a 5-day period (Blake and Zelinsky, 2018). Mechanism (2) was the main driver in flooding experienced in coastal areas of Mississippi and Louisiana during 2005 Hurricane Katrina, when a record 8.5-meter (27.8-foot) storm surge inundated Pass Christian, Mississippi (Knabb et al., 2005). Cangialosi et al. (2018) note potential Mechanism (3) flooding during 2017 Hurricane Irma, when downtown Miami experienced significant flooding due to the combined effects of heavy rainfall (305 mm [12 in.]

in 48 h) and inadequate drainage of urban runoff due to storm surge-elevated water levels 1.2 to 1.8 m (4 to 6 feet) above normal in the bay.

Flooding by Mechanism (3) has been noted in an increasing number of studies since 2010, when Bunya et al. (2010) and Dietrich et al. (2010) included riverine forcing (although steady in that study) in their hindcast simulations of 2005 Hurricanes Katrina and Rita. Potential impacts of under-prediction of water levels due to lack of rainfall-runoff forcing were noted by Bunya et al. (2010). Studies have also found interactions between rainfall-runoff and coastal flooding affecting large cities such as New York, Houston/Galveston and Jacksonville, Florida. Orton et al. (2012) recorded negative bias in predicted water levels when neglecting freshwater inputs for 2011 Hurricane Irene in the New York City metropolitan area. Additional studies in the Hudson River (Orton et al., 2015; Orton et al., 2018) continue to elucidate the importance of Mechanism (3) flooding, particularly in more upstream regions along a tidal river. For Houston/Galveston, Ray et al. (2011) compared the effects of steady versus unsteady HEC-RAS (Hydrologic Engineering Center River Analysis System) models forced with storm surge boundary conditions and found important effects of timing of the

* Corresponding author at: Department of Civil and Environmental Engineering, P.O. Box 5015, 1020 Stadium Drive, Cookeville, TN, USA.
E-mail address: akalyanapu@tnstate.edu (A.J. Kalyanapu).

peak storm surge and peak runoff in 2008 Hurricane Ike. [Torres et al. \(2015\)](#) investigated TC forcing of storm surge and rainfall-runoff specifically for the Houston Ship Channel under 2008 Hurricane Ike, 2012 Hurricane Isaac, and 2005 Hurricane Katrina conditions (using shifted landfall locations). When utilizing a coupled hydrology-hydrodynamic framework for their analysis, a typically small lag time (less than 24 h) between peak storm surge and peak rainfall-runoff was observed, indicating the potential for peak-on-peak flooding to occur under slightly shifted TC conditions. [Torres et al. \(2015\)](#) also determined that the location and angle of approach of TCs played an important role in the spatial distribution of precipitation and the associated runoff processes. Near Jacksonville, Florida, [Bacopoulos et al. \(2017\)](#) remarked that watershed runoff added 0.5 m to storm tide elevation in the lower St. Johns River and increased the inundated area by nearly 50% during 2008 Tropical Storm Fay. The wide geographic distribution of the collection of studies presented above demonstrates the potential importance of Mechanism (3) flooding across the Atlantic and Gulf coasts.

In each study where interactions between TC rainfall-runoff and storm surge were simulated, the effectiveness of modeling the interactions relied on the accuracy of the rainfall-runoff hydrographs generated, both in magnitude and in timing. While varied methods were used for routing runoff downstream, each method required accurate precipitation inputs as a prerequisite for adequately reproducing the observed runoff hydrographs. When hindcasting these events, modelers have the benefit of observed data for precipitation in many forms, from rain gage data to radar reflectivity. From these data, rainfall hyetographs can be synthesized to provide appropriate boundary conditions to hydrologic and hydraulic models, allowing reasonably accurate re-creation of flooding from both rainfall-runoff and storm surge contributions during past TC events. However, in typical coastal flood risk study methodologies, use of only historical data from particular past TCs, as in the Empirical Simulation Technique (EST, [Scheffner et al., 1999](#)), can fail to predict water levels generated by different TC parameters than observed, such as a different storm size, angle of approach, or intensity. By the use of historical data alone, an insufficient sample size can introduce too large of a sample error to adequately reproduce flood risk ([Toro et al., 2010; Divoky and Resio, 2007](#)).

As an alternative to the EST's use of historical storm parameters, the Joint Probability Method (JPM, [Myers, 1975](#)) develops a joint probability distribution of surge from the probability distributions of individual storm parameters (typically intensity, size, angle of approach, forward speed, and landfall location). A large number of hydrodynamic simulations is computed using the various combinations of parameters to approximate the multiple integral of the joint probability density function and establish a relationship between the parameters and the expected storm surge ([Toro et al., 2010](#)). The large number of simulations required to integrate numerically by brute-force is the main limitation of the JPM method. To reduce the amount of expensive computation necessary to solve the JPM problem by brute-force with high-fidelity hydrodynamic models (e.g. ADCIRC, the ADvanced-CIRCulation model by [Luettich and Westerink 2004](#)), Optimum Sampling (OS) methods were developed by [Resio \(2007\)](#) and further elucidated in [Toro et al. \(2010\)](#). These OS methods use either Bayesian quadrature or response-surface methods to approximate the JPM integral, and the methods substantially reduce the amount of computation required to achieve acceptable levels of accuracy. In the test of OS methods in [Toro et al. \(2010\)](#), surge results from 156 runs necessary for using OS-response surface and 158 runs for using OS-Bayesian quadrature were each compared with 2967 runs needed to solve the JPM integral by brute-force (a savings of 95%), and mean differences in surge were found near zero with standard deviations of about 0.15 m (0.5 ft). The authors of that study also note that additional refinement of models and an increase in parameter dimensionality will be needed to further reduce uncertainty in surge modeling, further increasing computational burdens due to the “curse of dimensionality”.

Although the addition of rainfall-runoff processes will incrementally

increase the computational cost of each run of coupled runoff-surge models compared with surge-only models, it is important to avoid exponential increases in computational cost of total runs required to solve the JPM integral that would be caused by increasing the number of simulation parameters (inducing the curse of dimensionality). An ideal situation would be gaining the ability to include rainfall-runoff processes without requiring any additional parameters at all. Fortunately, several parametric models exist for the spatial and temporal distribution of rain in TCs, some of which use only parameters that are already used in the JPM integral. To date, many one-to-one comparisons of parametric models have been carried out (in some cases against more dynamical than statistical models, see [Tuleya et al., 2007; Marchok et al., 2007](#) [henceforth “M7”]), but a single study has not aggregated all four of them to the authors' knowledge. Therefore, the objective of the current study is to *compare precipitation fields produced by four existing parametric TC rainfall models and then to select the most appropriate model for inclusion in future combined flooding studies*. In order to accomplish this objective, selected parametric TC rainfall models are used to simulate rainfall for Atlantic TCs from 2004 to 2017, and skill metrics are calculated for each model based on the resulting storm-total rainfall per M7. The models are then compared using each of the seven skill indices, which relate to the three key rainfall model characteristics established in M7: rainfall location pattern matching, mean rainfall and rain flux distributions, and extreme rain amounts.

2. Methodology

A total of six existing parametric models for TC rainfall were identified for consideration from the literature, listed below in chronological order:

1. Rain-Climatology and Persistence (henceforth “R-CLIPER”, see [Marks and DeMaria, 2003; Tuleya et al., 2007](#))
2. Interagency Performance Evaluation Task Force (IPET) Volume VIII Technical Appendix 8 (henceforth “IPET”, see [IPET, 2006](#))
3. Parametric Hurricane Rainfall Model (henceforth “PHRaM”, see [Lonfat et al., 2007](#); this model was modified by JTB to not include shear but only topographic effects)
4. Modified Smith for Rainfall (“MSR”, see [Langousis and Veneziano, 2009](#))
5. Risk Management Solutions, LTD. TC-Rain Model (“RMS”, see [Grieser and Jewson, 2012](#))
6. PDF Precipitation-Climatology and Persistence (henceforth “P-CLIPER”, see [Geoghegan et al., 2018](#))

Of the six models, a criterion for inclusion in this study was either that model code be readily available for use (ideally open-source) or could readily be reproduced from the literature. The authors were unable to locate existing code for any model, and the MSR and RMS models were not able to be reproduced from literature. Given the proprietary nature of the MSR and RMS models designed for commercial use, this is not surprising. Therefore, four models were used in this study: R-CLIPER, IPET, a modified version of PHRaM, and P-CLIPER. A brief description of each model is presented; for the full descriptions the interested reader is referred to the original publications. Units for the rainfall models are shown in formulae as they appeared in the publications from which they were taken. Where rain rate conversions to the standard for this study (millimeters per hour) took place, they are noted in the text. Where wind speeds appear, units of knots (abbreviated kts; 1 kt ≡ 0.5144 m/s) are used since the wind speeds are recorded in knots in both NHC's HURDAT2 best-track database and Colorado State University's EBTRK ([Demuth et al., 2006](#)).

2.1. R-CLIPER

The model was based on the work of [Lonfat et al. \(2004\)](#) and [Marks](#)

and DeMaria (2003), and a TC climatology from the Tropical Rain Measurement Mission (TRMM) satellite (Lonfat et al., 2004). Microwave imagery from TRMM was used to fit a curve from 482 TCs occurring globally between January 1, 1998 and December 31, 2002. The TRMM profiles for rain rates (TRR) were represented with several functions:

$$TRR(r, V) = \begin{cases} T_0 + (T_m - T_0)\left(\frac{r}{r_m}\right), & r < r_m \\ T_m e^{-\left(\frac{r-r_m}{r_e}\right)}, & r \geq r_m \end{cases} \quad (1)$$

with TRR as the rain rate in inches per day (necessitating a unit conversion in the current model), r as the radius from the center of the TC to the point of interest, V as the maximum wind speed, T_0 as the rain rate at the TC center $r = 0$ km and T_m as the maximum rain rate at $r = r_m$, where r_m is the radius from the center at which the maximum rain rate occurs. Another curve fit parameter was utilized, r_e , to specify the end behavior of the rainfall rate curves. A least-squares fit of the TRMM radial profiles found that the parameters could be represented as linear functions of the normalized maximum wind, U :

$$T_0 = a_1 + b_1 U \quad (2)$$

$$T_m = a_2 + b_2 U \quad (3)$$

$$r_m = a_3 + b_3 U \quad (4)$$

$$r_e = a_4 + b_4 U \quad (5)$$

where $U = 1 + \frac{V_m - 35}{33}$, and V_m is the maximum wind speed in knots, the unit used historically and operationally by the National Hurricane Center (NHC). The NHC operational version of R-CLIPER from Marks and Demaria (2003) used the values in Table 1 for the constants.

The input for this model is the storm track (including storm position as latitude and longitude, and the maximum wind speed V_{max} through time). This corresponds to JPM-OS parameters of storm landfall location, intensity, angle of approach, and forward speed (total of four parameters in JPM-OS style). It should be noted that R-CLIPER does not have an explicit size parameter such as radius of maximum winds (R_{max}), which could be used in JPM-OS-type studies; rather, the size of rainfall distribution is governed solely by the storm intensity.

2.2. IPET

The IPET model was based on the work of Lonfat et al. (2004) and Chen et al. (2006). The model computes mean rainfall intensity $m_I(r, \beta)$ with distance r (in kilometers) from the hurricane center to the point of interest and azimuth β (in degrees) relative to the direction of motion. Two components are considered: the symmetric component (i.e. the azimuthally-averaged component $m_I(r)$), and the asymmetric component (by including a factor). The symmetric component is estimated by assuming linear dependence of mean rainfall intensity at R_{max} on the central pressure deficit ΔP and fitting an exponential decay function with distance:

$$m_I(r) = \begin{cases} 1.14 + 0.12\Delta P; & r \leq R_{max} \\ (1.14 + 0.12\Delta P)e^{-0.3\left(\frac{r-R_{max}}{R_{max}}\right)}; & r > R_{max} \end{cases} \quad (6)$$

with m_I in millimeters per hour and ΔP in millibars. The asymmetric

component is estimated by multiplying the symmetric mean rainfall values by 1.5 for storms passing to the left of the sub-basin centroid (i.e. the rain is 50% more intense on the right-hand-side of the storm, appropriate for the northern hemisphere only). The inputs for this model are the storm position as latitude and longitude, the time, the radius of maximum winds R_{max} , and the central pressure deficit ΔP . All parameters can therefore be derived from the NHC storm track. The parameters correspond to the typical five JPM-OS parameters of landfall location, intensity, angle of approach, storm size, and forward speed. This model is more flexible in its ability to represent storms of varying size by including R_{max} . This capability comes at the cost of a fifth parameter (storm size), however, storm size is typically used in current JPM-OS studies already (IPET, 2006).

2.3. PHRaM

This model uses the rain rate estimates from R-CLIPER as a base and in its original formulation, adds two components to account for asymmetry (based on vertical wind shear) and orographic effects:

$$R_{PHRaM} = R_{R-CLIPER} + R_{shear\ mod} + R_{topography} \quad (7)$$

Based on Lonfat et al. (2007), the shear modification had an insignificant improving effect on Equitable Threat Score (ETS) for 2004 Atlantic landfalling storms, while incorporating both the topography and shear components resulted in significant ETS improvements across all rainfall thresholds. Given the additive nature of this model, it would seem that at least for the 2004 Atlantic landfalling storms, ignoring the shear component altogether might not have significant impact on rainfall estimates. Grieser and Jewson (2012) came to a similar conclusion and favored using orographic effects while parameterizing asymmetric rainfall re-distribution using storm motion rather than shear fields. Therefore, the rain rates were calculated in this study by the following formula:

$$R_{PHRaM} = R_{R-CLIPER} + R_{topography} \quad (8)$$

This modified version of the original PHRaM methodology is still referred to as PHRaM through the remainder of the text. In order to include the topography component, it was necessary to calculate the elevation gradient vector (which points in the steepest downslope direction) for each location in the simulation domain once in pre-processing, and also to calculate vector components of wind at each station for each timestep. The elevation gradients were calculated using the Slope and Aspect tools in Esri ArcGIS™ based on a raster dataset of elevation. The Slope tool was used to generate the magnitude of the slope in percent rise, which was divided by 100 to achieve a dimensionless slope. The Aspect tool was used to determine the direction of the steepest downhill slope, relative to north as 0 degrees and increasing clockwise. The original development of PHRaM used 10-km resolution elevation information due to the large geographic areas covered, so the same resolution of 10-km digital elevation models (DEM) was used for this study. Furthermore, a vector wind was also needed to estimate the orographic lifting component of rainfall:

$$R_{topography} = cV_s \cdot \nabla h_s = cw = c||V_s|||\nabla h_s||\cos(\theta) \quad (9)$$

where c = proportionality constant, V_s = 10 m vector wind field (m/s), ∇h_s = gradient of elevation (dimensionless), w = orography – induced updraft,

and θ = angle between downslope direction and wind direction (found in calculations as wind direction angle minus the downslope direction angle, in degrees).

According to Grieser and Jewson (2012), c varies whether the wind is propagating upslope or downslope such that the orographic component, $R_{topography}$, is as follows:

Table 1
Operational constants for R-CLIPER (2003).

Intercepts	Slopes
$a_1 = -1.10 \frac{\text{in}}{\text{day}}$	$b_1 = 3.96 \frac{\text{in}}{\text{day}}$
$a_2 = -1.60 \frac{\text{in}}{\text{day}}$	$b_2 = 4.80 \frac{\text{in}}{\text{day}}$
$a_3 = 64.5 \text{km}$	$b_3 = -13.0 \text{km}$
$a_4 = 150 \text{km}$	$b_4 = -16.0 \text{km}$

$$R_{topography} = \begin{cases} \frac{lift(m)}{100 m} \times R_{R-CLIPER} \\ = 1 \times slope \times \cos \theta \times R_{R-CLIPER}; \\ \text{upslope } \left(\begin{array}{l} V_s \cdot \nabla h_s \text{ is negative} \\ (\text{i.e. } |\theta| \geq 90^\circ) \end{array} \right) \\ \frac{-lift(m)}{20 m} \times R_{R-CLIPER} \\ = -0.2 \times slope \times R_{R-CLIPER} \times \cos \theta, \\ \text{downslope } \left(\begin{array}{l} V_s \cdot \nabla h_s \text{ is positive} \\ (\text{i.e. } |\theta| < 90^\circ) \end{array} \right) \end{cases} \quad (10)$$

where *lift* is defined as the elevation of the location in question minus the elevation of the steepest downslope point (in meters) and *slope* is the dimensionless change in elevation per distance as calculated in ArcGIS by taking one hundredth of the percent grade between two points. This would correspond to a tenfold increase in rain for a lift of 900 m (when including the original rainfall additively). The reason given by Lonfat et al. (2007) for the different upslope and downslope coefficients is to avoid negative rainfall solutions in the downslope regions, and this limitation is recognized in the case distinction. A further limitation is that *c* was calculated based on an elevation resolution of 10 km, and *c* would therefore need to be recalculated if a different resolution for elevation data were selected.

Inputs for the modified PHRaM model are the same as in R-CLIPER, except that a storm size parameter R_{max} is also required. This storm parameter is not used directly for simulating rainfall, but it is instead used to simulate the vector components of wind throughout the storm, in a parametric wind model similar to that used in ADCIRC with their NWS parameter set as 8 (Holland, 1980; Fleming et al., 2008). The component of wind being forced up- or down-slope was used to compute orographic adjustments to rainfall. To account for topography, a DEM for the study area was necessary to calculate slope and aspect, but the DEM is not a parameter *per se* for JPM-OS studies in the sense that it does not vary according to a defined probability distribution (implying that it would not change from scenario to scenario). Therefore, TC rainfall can be simulated using the modified no-shear PHRaM with the same five JPM-OS parameters as IPET.

2.4. P-CLIPER

Microwave imagery from TRMM was used to fit curves from 482 storms occurring globally between January 1, 1998 and December 31, 2002 for three intensity classifications: tropical storms (34–63 kts), Category 1–2 intensity (64–95 kts), and Category 3–5 intensity (> 95 kts). Since R-CLIPER (Lonfat et al., 2004; Marks and DeMaria, 2003) was built to generate mean rainfall intensities only, P-CLIPER was based around modifying the curve fits from R-CLIPER with exponential functions to reflect potential deviations from mean rainfall intensities by using a frequency *f* as an integer between –90 and 90 to scale the results. The equations are:

Tropical Storm (TS) intensity:

$$R(r, f) = \begin{cases} Ae^{Bf}, & r \leq 50km \\ \left(\begin{array}{l} 2.05957684 \times 10^{-5}r^2 \\ -1.672969851 \times 10^{-2}r \\ +3.838964806 \end{array} \right) e^{Bf}, & r > 50km \end{cases} \quad (11)$$

$$A = 2.995207, B = 0.027499$$

Category 1–2 (CAT12) intensity:

$$R(r, f) = \begin{cases} Ae^{Bf} * \frac{r}{30}, & r \leq 30km \\ \left(\begin{array}{l} -2.474340293 \times 10^{-9}r^4 \\ +1.935560971 \times 10^{-6}r^3 \\ -4.444507808 \times 10^{-4}r^2 \\ +6.840501651 \times 10^{-3}r \\ +6.656484399 \end{array} \right) e^{Bf}, & r > 30km \end{cases} \quad (12)$$

$$A = 5.539108, B = 0.021300$$

Category 3–5 (CAT345) intensity:

$$R(r, f) = \begin{cases} Ae^{Bf} * \frac{r}{30}, & r \leq 30km \\ \left(\begin{array}{l} -2.984284245 \times 10^{-7}r^3 \\ +3.033414728 \times 10^{-4}r^2 \\ -1.088545019 \times 10^{-1}r \\ +14.25059433 \end{array} \right) e^{Bf}, & r > 30km \end{cases} \quad (13)$$

$$A = 10.943440, B = 0.018433$$

According to one of the authors of the P-CLIPER model, in their original manuscript, the value 14.25059433 in the CAT345 curve fit was incorrectly transcribed as 1.425059433 and should be substituted where appropriate (Kevin Geoghegan, personal communication, 2018). The *A* values represent the rainfall rates at the center of the storm ($r = 0$ km) from the curve fits in Marks and DeMaria (2003). While *B* values were derived for Geoghegan et al. (2018), the derivation was not shown in their publication. It is important to note that a conversion from inches per day in Marks and DeMaria to millimeters per hour in Geoghegan et al. has taken place. All rain rates calculated in this study are reported in units of millimeters per hour.

Since over the history of a storm the intensity was allowed to change, the model as implemented selects the appropriate equation to use at each timestep based on the current storm intensity. In order to ensure uniformity of comparisons when the intensity fluctuates and to avoid spurious rainfall when a storm transitions rapidly between intensity classifications but not necessarily size, a uniform cutoff value of $r = 370$ km was used because this was the smallest cutoff of the three equations. For $r > 370$ km, the rainfall rate was considered zero (c.f. Geoghegan et al., 2018, which used a cutoff of 350 km).

The inputs for this model are the storm position as latitude and longitude, the time, the maximum wind speed V_{max} , and the departure from the average rainfall intensity (frequency), *f*. This adds an additional parameter for frequency, but since there is no explicit size parameter in P-CLIPER, there are still only five parameters needed for rainfall simulations, the same as the number of standard five JPM-OS parameters.

2.5. Development of code and comparison of model inputs

Each of the four models was coded into a Python script for simulation of TC rain given various storm tracks (“storm track files”) and a comma-separated list of latitude-longitude pairs at which to develop rainfall hyetographs (“station files”). The resulting Python script is available from the authors of this study upon request. A table of the inputs required is shown in Table 2. A uniform timestep of 15 min was used for all calculations in this study, since it was the greatest common factor between typical timesteps used in the constituent TC rainfall parametric models.

Each rainfall model simulates the rainfall rate at a given point in space at a particular time step. During any one time step, the rainfall rates are simulated at every point in the computational grid, and a time-history of the resulting rainfall rates is written for each grid point. Output produced therefore includes time-varying hyetographs at grid locations as comma-separated value files and as graphical representations produced using the matplotlib Python module. For simulations run using the modified PHRaM model, wind time-history files are also written as output.

2.6. Grid development

To set the computational grid extents, the storm tracks from 1988 to 2017 were imported from the Colorado State University Extended Best Track database (Demuth et al. 2006, henceforth EBTRK) into ArcGIS. Based on the validity extents of the models proposed above, these tracks

Table 2

Comparison of Model Inputs. **Bold** variables are constant with time for each simulation, but they must be specified at model start. Variables in lightface must be specified at each timestep. The variable “storm track” refers to latitude-longitude positions of the TC center at each timestep.

Model	Year	Required Inputs	Validity Radius (km)	Wind Validity (kts)	Accounts for Asymmetry?	Typical Timestep (hours)
R-CLIPER	2003	● storm track ● V_{max}	500	> 34*	No	0.5
IPET	2006	● storm track ● R_{max} ● ΔP	500	> 34*	Yes	N/A
PHRaM (modified from 2007 version)	2007	● storm track ● V_{max} ● RMW ● slope ● aspect	500	> 34*	Yes	0.25
P-CLIPER	2018	● storm track ● V_{max} ● frequency	370	> 34*	No	1

*assumed tropical storm (TS) relationship applied for storms with V_{max} less than 34 kts.

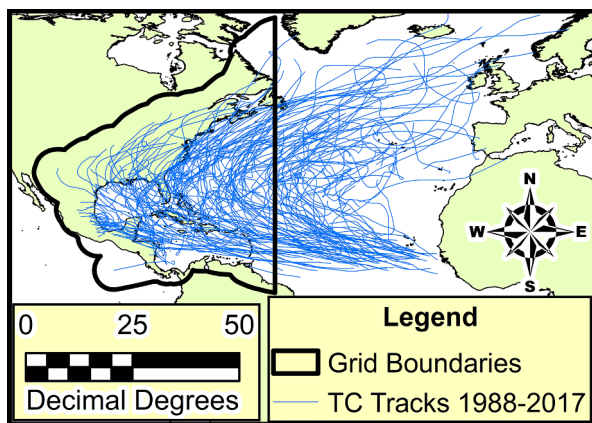


Fig. 1. Grid Extent Selection for Atlantic TC Rainfall.

were first transformed from discrete points to continuous lines, which were then buffered outwards 500 km. The region defined by this buffer, truncated on the east by the 60°W meridian, was used for setting all grid extents and is shown in Fig. 1.

The grid resolution was set as 0.1 degrees in both the longitudinal and latitudinal directions as a first step. A total of 222,327 points were needed to cover the domain in Fig. 1 at 0.1-degree spacing. The Generalized Bathymetric Chart of the Oceans (GEBCO, 2015) elevation raster, which incorporates Shuttle Radar Topography Mission (SRTM) 30-meter data over land, was used for elevation calculations. Prior to calculating the aspect and slope of the elevation grid points, the elevation raster was resampled to a 10-km spacing, per Lonfat et al. (2007). The slope and aspect values are used in the PHRaM calculation to determine orographic effects from topography; the spine of the Appalachian Mountains and the mountainous regions of Mexico can cause substantial orographic effects due to their relatively higher slope values (though only represented as 12–18% at 10-km resolution).

2.7. Storm track preparation

In order to evaluate and compare the four rainfall models, a library of the 221 TC tracks affecting the Atlantic basin from 2004 to 2017 was retrieved from the EBTRK database (Demuth et al., 2006). The EBTRK database improves upon the standard HURDAT2 format by including information on radius to maximum winds, which is necessary for the methodology proposed herein. The rainfall models require position/forward speed/approach angle (given as latitude-longitude pairs through time at 6-hour intervals), intensity (either as central pressure deficit ΔP or maximum winds V_{max}), and storm size (given as radius of

maximum winds R_{max}).

The 6-hourly positions were spline-interpolated to 15-minute intervals. The central pressure deficit was defined as:

$$\Delta P = POCI - MSLP \quad (14)$$

While the majority of the pressure information from EBTRK was readily converted to central pressure deficits using the ADCIRC convention of far-field pressure as 1013 mbar (mb), some recorded central pressures were greater than 1013 mb (103 records, 27 unique storms) and were defined as 1013 mb to be consistent with climatological means for the Atlantic. Missing central pressure deficit records were persisted from the closest timestep for which data was available.

While the majority of the R_{max} information was provided in the database, some gaps existed but needed to be filled prior to modeling the rainfall with either IPET or PHRaM.

If no R_{max} information had been recorded for the storm before (after) a given timestep, the R_{max} at the first (last) available timestep was persisted backwards (forwards) to fill the gaps; when data was available both prior to and following a missing data point, linear interpolation in time was used.

The R_{max} gap-filling methodology is potentially flawed if a storm undergoes extratropical transition and dramatically changes shape (e.g. 2012 Hurricane Sandy). Since 83 of the original 221 storms undergo extratropical transition at some point during their track, further study is necessary to determine the impacts on precipitation.

Of the 221 Atlantic TCs from 2004 to 2017, only 67 produced rainfall over the continental United States (CONUS) while the storms' best tracks were recorded by NHC. This approach neglected storms not producing rainfall over CONUS, and it also removed the influence of Eastern Pacific TCs affecting CONUS. It is also the reason that two 2015 Atlantic TCs were excluded: while TS Erika (2015) and TS Grace (2015) both have rainfall attributed to CONUS from their remnants, the NHC tracks do not extend into the time period during which the rain fell, so these storms were removed from consideration by the current methodology. To consider storms where the NHC track ended before the rainfall record, the storm tracks were truncated to ensure that only the inclusive time where both rain and NHC track were defined was simulated for rainfall comparisons. These truncations are unlikely to affect landfall statistics (except when a storm's NHC track ends before the system comes ashore), but they may have substantial impacts on the total rainfall statistics later in the storms' lifetimes after landfall. Of the 67 storms affecting CONUS with rainfall while having a defined NHC track, 20 (30%) have both modelled and observed rain which potentially occurred but has been truncated from the analysis since the rain occurred prior to NHC defining a track for the storm. Similarly, 54 of the 67 storms affecting CONUS with rainfall have some rainfall truncated from the end of both the modelled and observed scenarios due to

Table 3

Simulated Storms and Constraints on Simulation Time. **Boldface** indicates the storm was a tropical cyclone of hurricane intensity (> 64 kts) at CONUS landfall, while lightface indicates tropical depressions and tropical storms; intensity at CONUS landfall(s) is(/are) given in parentheses. For storms not making CONUS landfall as a tropical cyclone but producing rain over CONUS, maximum intensity and storm name are given in italics. Data are retrieved from the NOAA reports for each storm (<https://www.nhc.noaa.gov/data/tcr/>).

Year	Name	Simulation Start	Simulation End	Max. Total Rain* (mm)
2004	ALEX (105)	1800 UTC 31 Jul 2004 ^T	1200 UTC 5 Aug 2004 ^R	192
	BONNIE (40)	1200 UTC 11 Aug 2004 ^R	0000 UTC 14 Aug 2004 ^T	154
	CHARLEY (130, 125, 70, 65)	1200 UTC 12 Aug 2004 ^R	1200 UTC 15 Aug 2004 ^T	251
	FRANCES (90, 50)	1200 UTC 3 Sep 2004 ^R	1800 UTC 10 Sep 2004 ^T	599
	GASTON (65)**	1200 UTC 27 Aug 2004 ^T	1200 UTC 2 Sep 2004 ^R	320
	HERMINE (35)**	1800 UTC 27 Aug 2004 ^T	1200 UTC 31 Aug 2004 ^T	320
	IVAN (105, 30)	1200 UTC 13 Sep 2004 ^R	0600 UTC 24 Sep 2004 ^T	432
	JEANNE (105)	1200 UTC 25 Sep 2004 ^R	1200 UTC 29 Sep 2004 ^T	304
	MATTHEW (35)	1200 UTC 8 Oct 2004 ^T	0600 UTC 11 Oct 2004 ^T	457
	ARLENE (50)	1800 UTC 8 Jun 2005 ^T	0600 UTC 14 Jun 2005 ^T	250
2005	CINDY (65, 45)	1200 UTC 4 Jul 2005 ^R	0600 UTC 11 Jul 2005 ^T	241
	DENNIS (105)	1200 UTC 7 Jul 2005 ^R	0600 UTC 18 Jul 2005 ^T	325
	EMILY (140)	1200 UTC 19 Jul 2005 ^R	1200 UTC 21 Jul 2005 ^T	132
	KATRINA (70, 110, 105)	1200 UTC 24 Aug 2005 ^R	0600 UTC 31 Aug 2005 ^T	417
	OPHELIA (75)	0600 UTC 6 Sep 2005 ^T	1200 UTC 17 Sep 2005 ^R	445
	RITA (100)	1200 UTC 20 Sep 2005 ^R	0600 UTC 26 Sep 2005 ^T	406
	TAMMY (45)	0600 UTC 5 Oct 2005 ^T	0000 UTC 7 Oct 2005 ^T	368
	WILMA (105)	1200 UTC 22 Oct 2005 ^R	1200 UTC 25 Oct 2005 ^R	337
	ALBERTO (40)	1200 UTC 11 Jun 2006 ^R	1200 UTC 16 Jun 2006 ^R	182
	BERYL (45)	1200 UTC 18 Jul 2006 ^{R T}	1200 UTC 22 Jul 2006 ^{R T}	8
2006	ERNESTO (40, 40, 60)	1200 UTC 30 Aug 2006 ^R	0600 UTC 4 Sep 2006 ^T	371
	ANDREA (50)	1200 UTC 9 May 2007 ^R	1200 UTC 12 May 2007 ^R	20
	BARRY (30)	0000 UTC 31 May 2007 ^T	1200 UTC 5 Jun 2007 ^T	203
	ERIN (30)	0000 UTC 15 Aug 2007 ^T	1800 UTC 19 Aug 2007 ^T	325
	GABRIELLE (50)	0000 UTC 8 Sep 2007 ^T	0600 UTC 11 Sep 2007 ^T	229
	HUMBERTO (80)	0600 UTC 12 Sep 2007 ^T	1200 UTC 14 Sep 2007 ^T	359
	NOEL (70)	1200 UTC 30 Oct 2007 ^R	1200 UTC 5 Nov 2007 ^R	128
	OLGA (50)	1200 UTC 13 Dec 2007 ^R	0600 UTC 16 Dec 2007 ^T	180
	CRISTOBAL (55)	0000 UTC 19 Jul 2008 ^T	0600 UTC 23 Jul 2008 ^T	202
	DOLLY (75, 70)	1200 UTC 22 Jul 2008 ^R	0000 UTC 27 Jul 2008 ^T	381
2007	EDOUARD (55)	1200 UTC 4 Aug 2008 ^R	1800 UTC 6 Aug 2008 ^T	165
	FAY (50, 55, 55, 45)	1200 UTC 17 Aug 2008 ^R	0600 UTC 28 Aug 2008 ^T	702
	GUSTAV (90)	1200 UTC 29 Aug 2008 ^R	1200 UTC 5 Sep 2008 ^T	533
	HANNA (60)	1200 UTC 4 Sep 2008 ^R	1200 UTC 8 Sep 2008 ^{R T}	245
	IKE (95)	1200 UTC 8 Sep 2008 ^R	1200 UTC 15 Sep 2008 ^R	480
	BILL (60)†	1200 UTC 22 Aug 2009 ^R	1200 UTC 25 Aug 2009 ^R	135
	CLAUDETTE (40)	0600 UTC 16 Aug 2009 ^T	1800 UTC 17 Aug 2009 ^T	149
	IDA (90)	1200 UTC 10 Nov 2009 ^R	0600 UTC 11 Nov 2009 ^T	457
	ALEX (95)	1200 UTC 29 Jun 2010 ^R	0000 UTC 2 Jul 2010 ^T	890
	BONNIE (35)	0600 UTC 22 Jul 2010 ^T	1800 UTC 25 Jul 2010 ^T	146
2010	EARL (125)	1200 UTC 2 Sep 2010 ^R	1200 UTC 5 Sep 2010 ^R	131
	HERMINE (60)	1800 UTC 4 Sep 2010 ^T	0000 UTC 10 Sep 2010 ^T	416
	IGOR (135)†	1200 UTC 20 Sep 2010 ^R	1200 UTC 22 Sep 2010 ^R	238
	NICOLE (40)	0000 UTC 28 Sep 2010 ^T	1200 UTC 30 Sep 2010 ^R	323
	DON (30)	0600 UTC 27 Jul 2011 ^T	0600 UTC 30 Jul 2011 ^T	65
	IRENE (75, 60, 55)	1200 UTC 24 Aug 2011 ^R	0000 UTC 30 Aug 2011 ^T	400
	LEE (40)	0000 UTC 2 Sep 2011 ^T	1800 UTC 6 Sep 2011 ^T	532
	BERYL (55)	1200 UTC 25 May 2012 ^T	1200 UTC 31 May 2012 ^R	381
	DEBBY (35)	1200 UTC 23 Jun 2012 ^T	1200 UTC 27 Jun 2012 ^T	731
	ISAAC (70, 70)	1200 UTC 25 Aug 2012 ^R	0600 UTC 1 Sep 2012 ^T	678
2011	SANDY (100)	1200 UTC 24 Oct 2012 ^R	1200 UTC 31 Oct 2012 ^T	326
	ANDREA (50)	1800 UTC 5 Jun 2013 ^T	1800 UTC 8 Jun 2013 ^T	362
	KAREN (55)	0600 UTC 3 Oct 2013 ^T	0600 UTC 6 Oct 2013 ^T	286
	ARTHUR (85, 85)	1800 UTC 28 Jun 2014 ^T	1200 UTC 6 Jul 2014 ^R	222
	ANA (40)	0600 UTC 6 May 2015 ^T	1800 UTC 12 May 2015 ^T	175
	BILL (50)	0000 UTC 16 Jun 2015 ^T	0000 UTC 21 Jun 2015 ^T	384
	ERIKA (45)***	—	—	229
	GRACE (50)***	—	—	275
	BONNIE (30)	1800 UTC 27 May 2016 ^T	1200 UTC 3 Jun 2016 ^R	354
	COLIN (45)	1200 UTC 5 Jun 2016 ^T	0600 UTC 7 Jun 2016 ^T	446
2016	HERMINE (70)	1800 UTC 28 Aug 2016 ^T	0600 UTC 3 Sep 2016 ^T	568
	JULIA (30)	0600 UTC 13 Sep 2016 ^T	1800 UTC 18 Sep 2016 ^T	165
	MATTHEW (75)	1200 UTC 4 Oct 2016 ^R	0600 UTC 9 Oct 2016 ^T	481

(continued on next page)

Table 3 (continued)

Year	Name	Simulation Start	Simulation End	Max. Total Rain* (mm)
2017	CINDY (45)	1800 UTC 19 Jun 2017 ^T	0600 UTC 24 Jun 2017 ^T	475
	EMILY (50)	1800 UTC 30 Jul 2017 ^T	1200 UTC 1 Aug 2017 ^R	183
	HARVEY (115, 105, 40)	1200 UTC 25 Aug 2017 ^R	1200 UTC 2 Sep 2017 ^T	1539
	PTC10 (40)	1800 UTC 27 Aug 2017 ^T	1800 UTC 29 Aug 2017 ^T	479
	IRMA (115, 100)	1200 UTC 8 Sep 2017 ^R	1200 UTC 13 Sep 2017 ^T	550
	JOSE (135)	1200 UTC 18 Sep 2017 ^R	1200 UTC 24 Sep 2017 ^R	165
	NATE (75, 65)	1200 UTC 4 Oct 2017 ^R	1200 UTC 10 Oct 2017 ^R	252
	PHILIPPE (35)	1200 UTC 28 Oct 2017 ^R	0000 UTC 29 Oct 2017 ^T	278

*: recorded rainfall amount is per WPC and may not match simulation rain.

**: 2004 Gaston and 2004 Hermine were not separated in rainfall analysis by NHC.

***: storm was not simulated since NHC track and recorded rainfall do not overlap at all.

†: no observed rainfall over CONUS.

^R: length of rainfall constrained simulation length.

^T: length of storm track constrained simulation length.

the storm persisting (and continuing to produce rainfall) after NHC tracking responsibility ceased. The controlling data availability for each of the simulated storms is shown in Table 3.

2.8. Observed data

In order to compare the models' capability of reproducing observed rainfall patterns, the National Stage IV Quantitative Precipitation Estimates (QPE) files for CONUS were downloaded from the University Corporation for Atmospheric Research (UCAR). UCAR maintains the Stage IV QPE for the period of record from 2002 through the present in standard GRIBbed Binary (GRIB1 and GRIB2) format at 1-hour, 6-hour, and 24-hour intervals (Lin, 2011). 6-hourly GRIB files covering the appropriate dates from 2004 to 2017 were downloaded and converted to the GRIB2 format if necessary. Although these observations are originally on the polar stereographic Hydrologic Rainfall Analysis Projection (HRAP, Reed and Maidment, 1999) grid, they were interpolated to 0.1-degree resolution on a regularly-spaced latitude-longitude grid to roughly match the resolution used by Lonfat et al. (2007) and by M7. This was accomplished using the WGRIB tools by Wesley Ebisuzaki (available from <http://www.cpc.ncep.noaa.gov/products/wesley/wgrb.html>). A budget interpolation scheme was used to preserve the integral of rain flux when changing grid resolutions, as opposed to a bilinear interpolation of point maximum values. After careful analysis of overlap of storm track and rainfall affecting CONUS, the appropriate 6-hourly files to sum for each storm were aggregated into storm-total observed precipitation datasets.

2.9. Model runs

After the storm track and grid inputs had been prepared, along with the observed data, 10 runs of each storm were computed for a total of 670 runs:

- 1 for each storm using R-CLIPER
- 1 for each storm using IPET
- 1 for each storm using PHRaM
- 7 for each storm using P-CLIPER (varying f over $-90, -60, -30, 0, +30, +60$, and $+90$)

The variation of f was intended to explore the full range of possibilities for the P-CLIPER model. No calibration of f or any other parameter is undertaken in this study; instead the models are used with the parameters originally published by their respective authors, as optimized during their respective model developments.

2.10. Statistical measures of model skill

Using the storm-total rainfall for grid points within 10 km of land (thereby ignoring rain over open ocean), metrics of model skill were calculated for the 2004–2017 Atlantic TCs in Table 3 per M7. These metrics and the attribute of the precipitation field measured are summarized in Table 4 (adapted from M7). Each metric is defined in detail in M7.

In order to calculate equitable threat score (ETS), contingency tables were calculated for the number of hits, misses, false alarms, and correct rejections that each model made regarding storm-total rainfall above a certain threshold. Definitions for each term are shown in the mock contingency table, Table 5.

3. Results

Model skill scores based on the metrics in Table 4 are presented for the 2004–2017 Atlantic TCs producing rainfall over CONUS. Remarks about the ability of each model to capture the rainfall produced by a TC like 2017 Hurricane Harvey are also presented.

3.1. 2004–2017 Atlantic TCs affecting CONUS

3.1.1. Pattern matching

The ability of each model to match locations of storm-total rainfall was evaluated using the equitable threat score and correlation between rain patterns. To estimate effects of grid resolution on results in a hydrologic fashion, the storm-total rainfall values were budget-interpolated from the original 0.1-degree resolution to Hydrologic Unit Code (HUC)-10 areas near the coastline, shown in Fig. 2.

Table 4

Individual TC QPF skill indices and primary QPF attribute described. Adapted from Marchok et al. (2007), © American Meteorological Society. Used with permission.

Index	QPF Attribute Described		
	Location Pattern	Mean/Median/ Volume	Extreme Rain
Large-scale ETS	X		
Pattern correlation	X		
Mean rainfall error index		X	
Large-scale CDF median value		X	
Track-relative CDF median value		X	
Large-scale CDF percentage at 95th percentile			X
Track-relative CDF percentage at 95th percentile			X

Table 5
Contingency Table for Calculation of Model Skill Statistics.

Forecast (predicted by model)	Observed	
	Yes	No
Yes	Hits (YY) model > threshold observed > threshold	False Alarms (YN) model > threshold observed < threshold
No	Misses (NY) model < threshold observed > threshold	Correct rejections (NN) model < threshold observed < threshold

The average HUC-10 area covered approximately 550 square kilometers, while the original resolution covered about 105 square kilometers per cell area. Plots of ETS for the 2004–2017 Atlantic TCs producing rain over CONUS at grid points within 500 km of each storm track are shown in Fig. 3, which is divided into two panels representing the two grid resolutions (regularly-spaced 0.1-degree resolution and irregularly-spaced HUC-10 units near the coastline).

The rainfall thresholds for the ETS plots in Fig. 3 and all subsequent figures were as specified in M7 using the decibel rain rate (dBR) in inches:

$$dBR = 10 \log_{10}(R) \quad (15)$$

where R is the value of the rain flux threshold and dBR takes values over: $\{-30, -10, -9, -8, -7, \dots, 13, 14, 15\}$. These thresholds were converted to millimeters for this study.

With regards to large-scale ETS, the IPET model outperforms any other model as storm-total rainfall threshold increases above 76.2 mm (3 in.), on both high and low resolutions. The PHRaM results are very similar to R-CLIPER. This indicates that the additional computational expense incurred by using PHRaM may not yield substantially better results for the 2004–2017 climatology on average. There is considerable increase in ETS when relaxing the location dependency by interpolating data to the coarser HUC10 grid. For example, at a rainfall threshold of 127.3 mm (5 in.), the ETS for IPET is 0.16 in panel (A) of Fig. 3 (the high-resolution portion), while the ETS for IPET improves to 0.27 in panel (B) of Fig. 3 (the low-resolution HUC-10 evaluation). Based on frequency bias (average of 1.25 over all rain thresholds compared with 0.48 for R-CLIPER, plot not shown), IPET appears to consistently over-predict the rates of occurrence of rain above given thresholds of storm-total rainfall. P-CLIPER (with $f = 30, 60$, and 90)

are the only models in this study producing storm-total amounts in excess of 506.7 mm (20 in.). The location-based correlations between modeled and observed storm-total rain were also calculated. Plots of the absolute value of the individual storm-total Pearson correlations with the observed totals are shown in Fig. 4.

IPET produces mixed results when correlating observed data with simulated; it has the highest correlation of all models for 46% of cases (31 of 67) but also the lowest correlation of all models for 39% of cases (26 of 67). It should be noted that only 67 cases are presented here; 2010 Hurricane Igor, which produced 238 mm rainfall over 48 h in St. Lawrence, Newfoundland, was present in the WPC analyses but was outside the coverage of the Stage IV observed product. When considering all storms together, the correlation coefficients are presented in Fig. 5.

In the overall case, the IPET model produces results that are significantly more correlated with observed data than any other model, based upon non-overlap of the 99% confidence intervals for Pearson correlation. There is no significant difference in correlation among P-CLIPER variants of $f = 0, 30, 60$, and 90 , while P-CLIPER with $f = -30$ and R-CLIPER are correlated similarly to each other. PHRaM and P-CLIPER with $f = -60$ tie for fourth place, while P-CLIPER with the low value of $f = -90$ is the least correlated to the observed data.

3.1.2. Mean rainfall and rain flux distributions

In order to compare each model's ability to produce heavy, medium, and light rainfall amounts at varying radii, the mean storm-total rainfall was plotted as a function of radius from the track of the TC center in Fig. 6. In the inner-core region, P-CLIPER with $f = 90$ produces values approximately ten times greater than observed, indicating the severity of the maximum rainfall P-CLIPER can produce. For radii less than 250 km, the observed values fall between the P-CLIPER curves $f = 0$ and $f = 30$, indicating that the single f -value providing the best fit to the observed mean storm-total rainfall profile for 2004–2017 would be represented by a positive f -value in that range. However, as radii increases beyond 370 km, P-CLIPER was not configured to produce rainfall while the observed profile continues to produce 15–20 mm. Similar to earlier observations based on frequency bias, the IPET model tends to over-predict storm-total rainfall at radii less than 425 km; beyond 425 km, IPET also under-predicts storm-total rainfall. R-CLIPER and PHRaM have a pronounced low bias in mean storm-total rainfall at all radii. The mean rainfall distribution of each model was used to calculate the mean rainfall error index (MREI) over each 20-km band out to 400 km, as in M7.

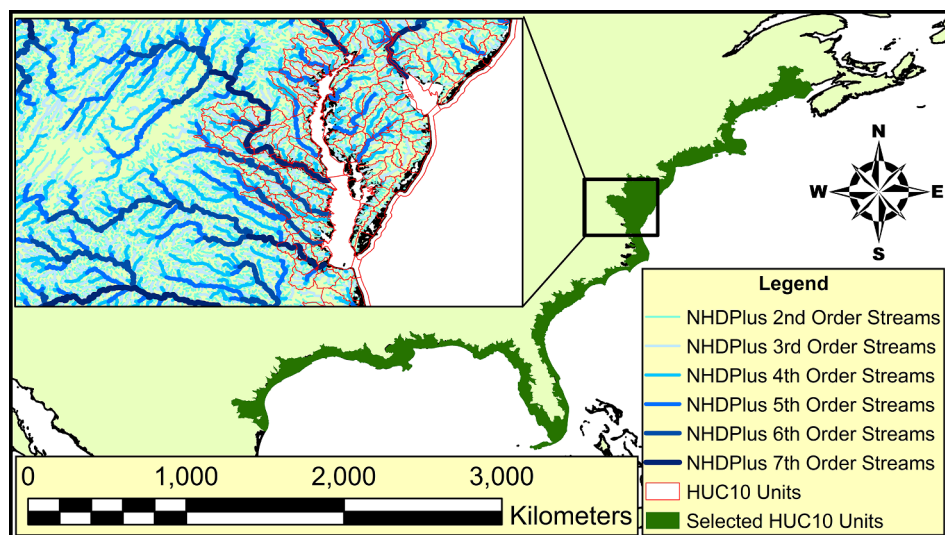


Fig. 2. HUC10 Units Selected for Analysis. The National Hydrography Dataset Plus (NHDPlus) version 1.2 streams are shown in the inset, with heavier shades representing increasing stream order. The red outlines represent HUC10 units. For references to color, the reader is referred to the web version of this article.

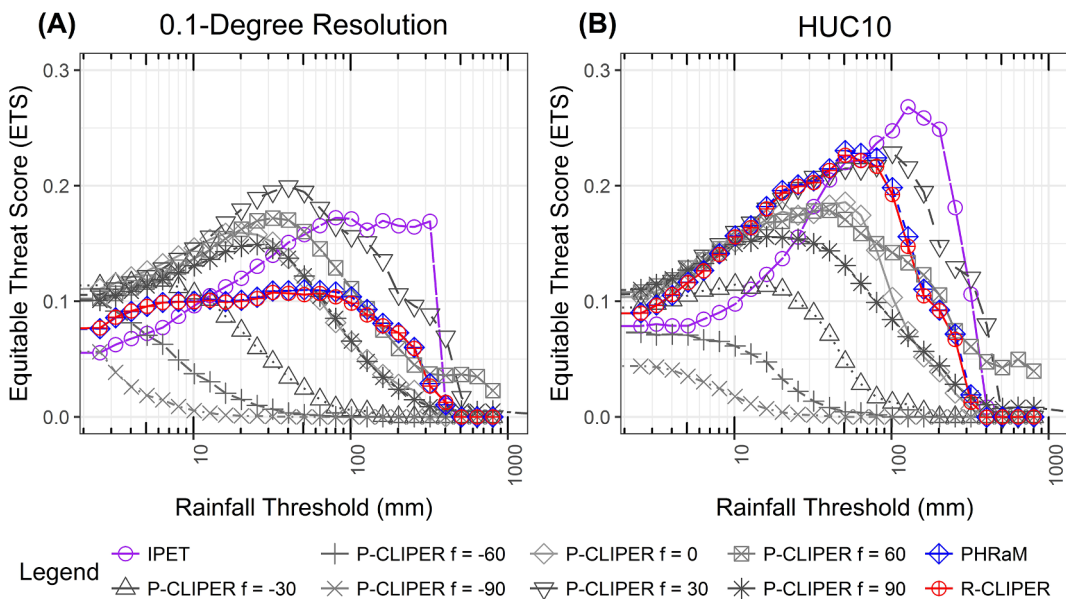


Fig. 3. 2004–2017 US-Mainland Storms Equitable Threat Score on varied resolution grids. Panel (A) is a regularly-spaced latitude-longitude grid, while Panel (B) is irregularly-spaced due to HUC10 boundaries.

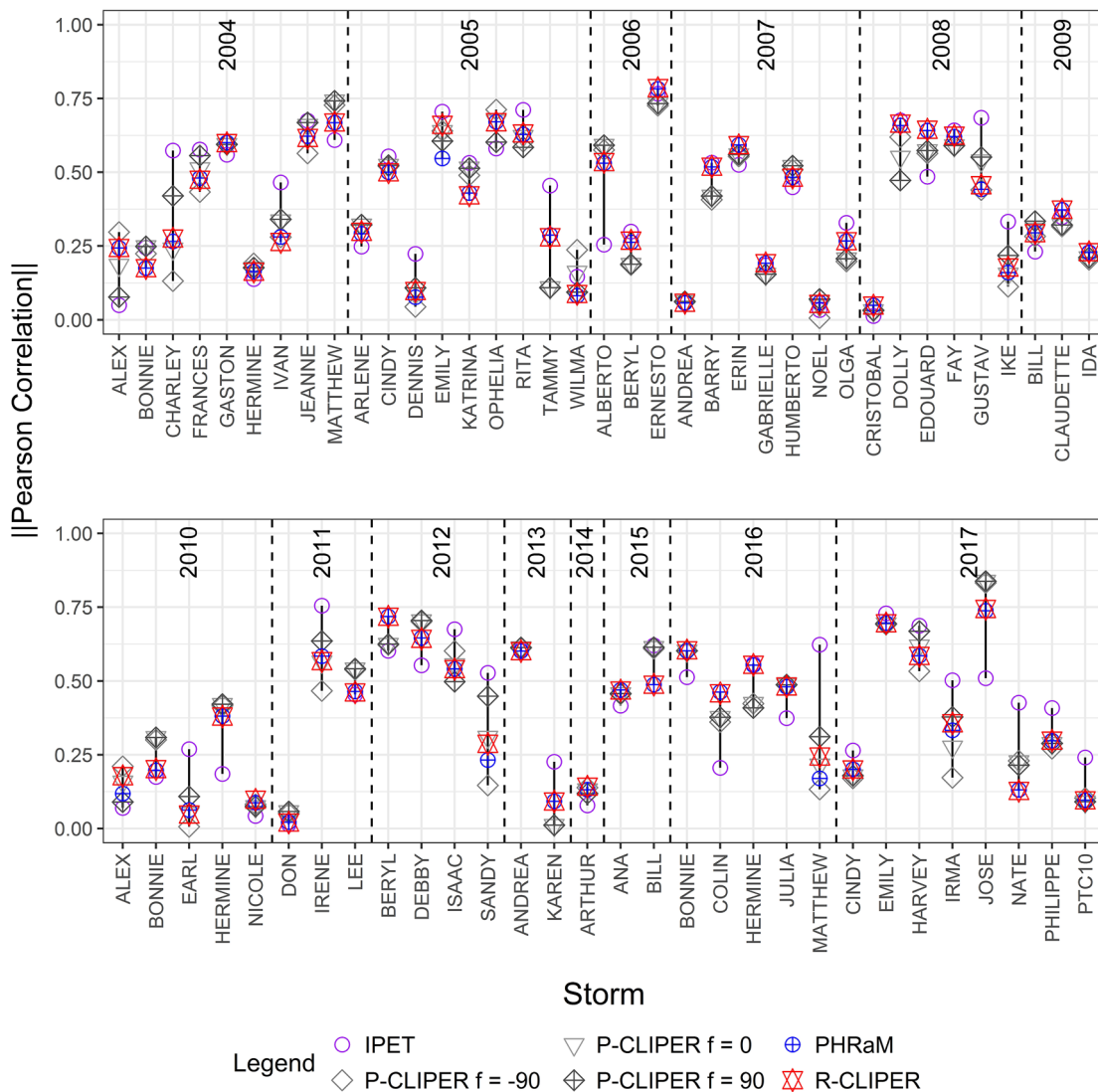


Fig. 4. QPF pattern correlation with observed Stage IV QPE for storm-total rainfall for selected models and all CONUS Atlantic TCs from 2004 through 2017.

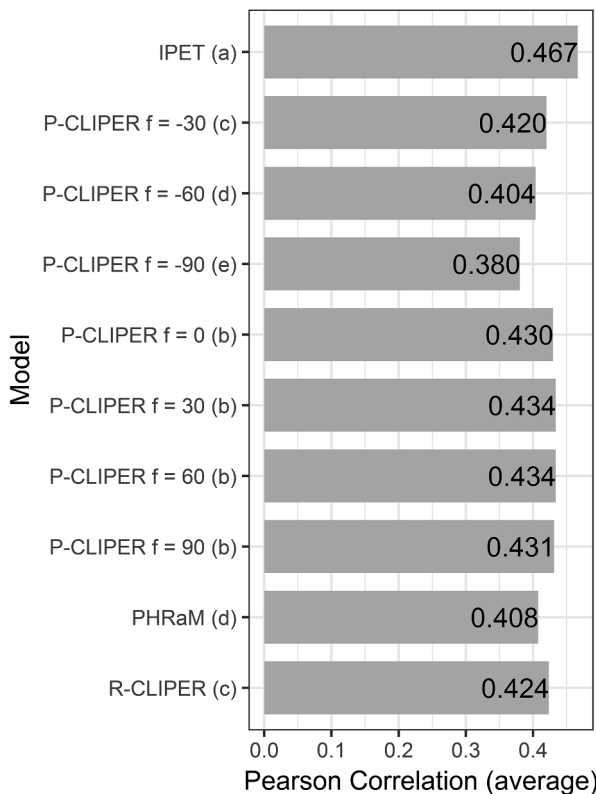


Fig. 5. Pearson Correlations averaged over all studied storms 2004–2017. Letters in parentheses indicate statistically similar groups based on 99% confidence intervals of correlation calculated using Fisher's Z-transformation.

Since this study focuses on ability to simulate TC rainfall-runoff flooding processes, the total rain volume produced in each storm was calculated and plotted in Fig. 7. P-CLIPER variants were not plotted due to their large range of volumes attainable by tuning f sufficiently large or small: using P-CLIPER, the lowest non-zero value of volume for a

given storm was 0.02 cubic kilometers in 2009 TS Bill with $f = -90$, and the highest volume produced was up to 158.63 cubic kilometers in 2008 TS Fay with $f = 90$. It should also be noted that in this study, TS Fay was simulated for 258 h, which is in the 94th percentile of simulation lengths for storms in this study (equaled or surpassed only by simulating 2004 Hurricane Ivan for 258 h, 2005 Hurricane Dennis for 258 h, and 2005 Hurricane Ophelia for 270 h). The length of simulation may play an outsized role in storm-total rainfall when using P-CLIPER. In addition to by-storm volumes, the average case including all storms was also computed to elucidate any consistent biases in rain volume and is shown in Table 6.

Overall, the IPET model and P-CLIPER models with $f \geq 30$ produce too much rainfall volume on average, from as little as 18% high bias to producing almost six times the observed volume. The other models, including PHRaM and R-CLIPER, produce far too little rainfall volume in the average case, with typical low bias for PHRaM and R-CLIPER indicating a failure to predict nearly half the rainfall volume. For engineering purposes, it is preferable to use a model which is biased slightly higher rather than lower when forced to choose between two models in order to ensure conservative results, so the IPET model would be selected based on the rainfall volume basis. Alternatively, since P-CLIPER can be tuned to nearly any desired volume, as shown by the wide range of bias (−95% to +483% of observed) in Table 6, the P-CLIPER model could be selected for its ability to match historical observations and development of an appropriate site-specific distribution of f would be necessary. It is also important to note that while the total volume may be predicted fairly well by some models in certain storms (e.g. IPET in 2017 Harvey, Fig. 7), the placement of this rain volume is also paramount to accurate flood predictions, so the previous location-based metrics of ETS and pattern correlation should also be considered.

In order to compare the relative occurrences of storm-total rainfall above each threshold, the probability distribution functions (PDF) and cumulative distribution functions (CDFs) of storm-total rainfall are plotted in Figs. 8 and 9, respectively.

Compared with the observed PDF, IPET generally predicts slightly more frequent amounts of rainfall at each threshold. P-CLIPER variants with f greater than or equal to 30 also predict higher frequencies at

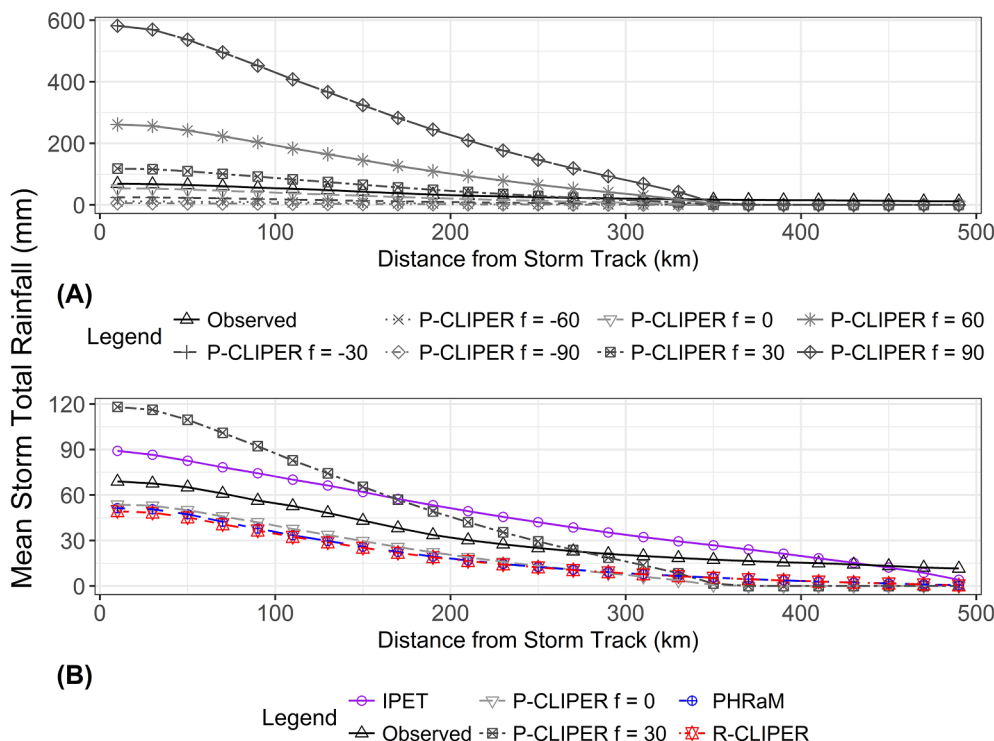


Fig. 6. Mean storm-total rainfall vs. distance from track for the 2004–2017 Atlantic TCs producing rainfall over CONUS. (A) presents variations of the P-CLIPER f -values. (B) presents the other models, as well as the two P-CLIPER variants most closely matching the observed pattern. Note the different vertical scales in (A) and (B).

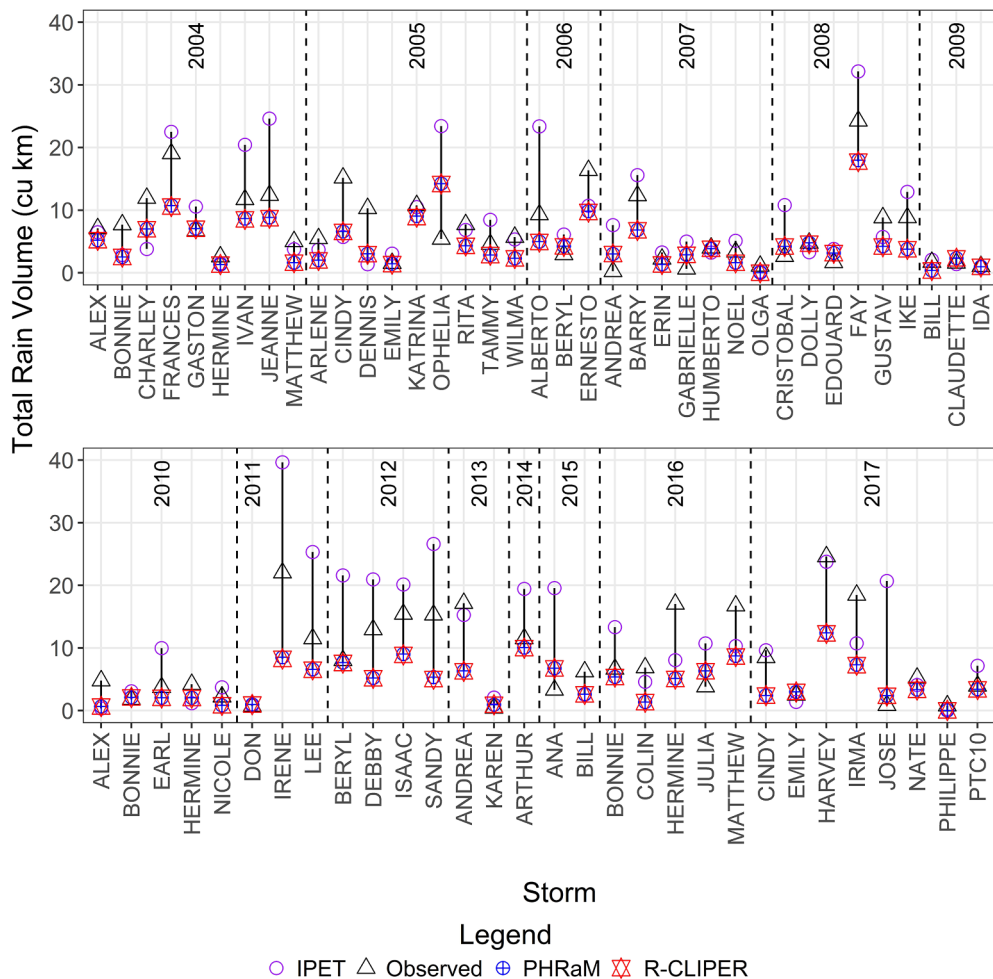


Fig. 7. Total rain volume (cubic kilometers) within 500 km of storm track for each storm and model, excluding P-CLIPER variants.

Table 6

Rainfall volume statistics for all points within 500 km of storm track.

	IPET	PHRaM	R-CLIPER	Observed			
Volume per case (km^3)	70.9	27.7	26.8	51.7			
Mean rainfall bias (km^3)	19.2	-24.0	-24.9	-			
Rainfall bias (%)	37%	-46%	-48%	-			
P-CLIPER							
	f = -90	f = -60	f = -30	f = 0	f = 30	f = 60	f = 90
Volume per case (km^3)	2.7	5.8	12.7	27.7	61.0	135.3	301.3
Mean rainfall bias (km^3)	-49.0	-45.9	-39.0	-24.0	9.3	83.6	249.6
Rainfall bias (%)	-95%	-89%	-76%	-46%	18%	162%	483%

thresholds above 20.2 mm (0.8 in.). R-CLIPER and PHRaM predict too much light rain (below 10 mm) and not enough heavier rain. These trends are also evident in Fig. 9.

The values for 50th percentile (median) of rain flux from the CDFs were compared from each model and the observed data. The Stage IV data within 500 km produced a median value at 4.5 mm, and the median values for IPET and P-CLIPER ($f = 30, 60, 90$) were higher than observed by up to a factor of 10, indicating a potential for producing too much rainfall at higher thresholds. Similarly, R-CLIPER, PHRaM, and P-CLIPER variants with f -values of zero or less had median values lower than observed by as much as a factor of 10, indicating that the models produce too little rainfall in the higher thresholds. The median values were used to calculate the large-scale and track-relative CDF

median value indices as detailed in M7.

The PDF and CDF of storm-total rainfall were also plotted for 100-km bands ranging from 0 km to 500 km away from the storm track (e.g. 0–100 km, 300–400 km). Per M7, the 0–100 km band would mostly capture rain in the eyewall (or its remnants), with larger radii bands typically representing contributions from outer rainbands and stratiform rain. The 0–100 km band PDF and CDF are shown in Figs. 10 and 11.

In the inner-core 0–100 km region, the track-relative CDF distributions are extremely similar to the large-scale versions, except that median values are generally at higher rainfall thresholds (typical increase of 164% from large-scale). The PHRaM/R-CLIPER models slightly over-predict the low rainfall amounts below 10 mm and

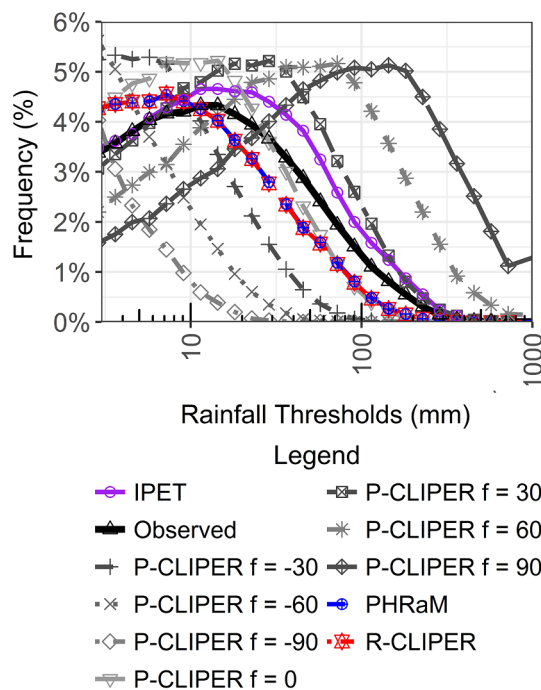


Fig. 8. Rainfall probability distribution functions (PDF) of rain flux within 500 km of the observed storm tracks for 2004–2017 Atlantic TCs producing rain over CONUS. Only rainfall thresholds in excess of 2.54 mm (0.1 in) are shown.

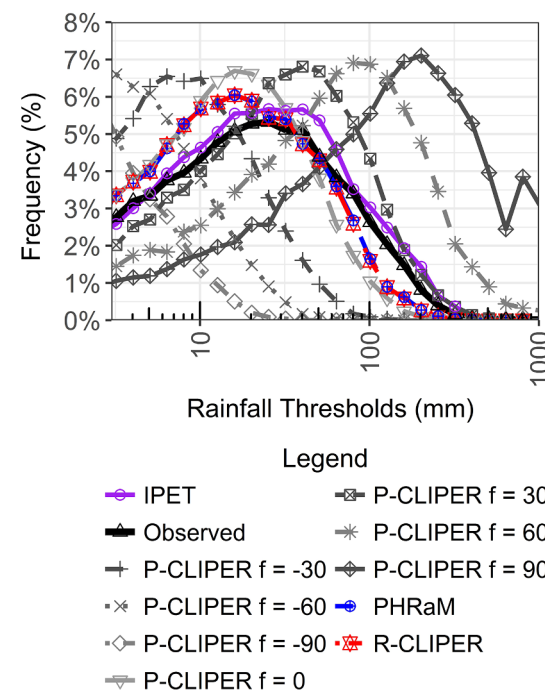


Fig. 10. PDF of rainfall within 100 km of the storm track for all models and observations of 2004–2017 Atlantic TCs producing rainfall over CONUS. Only rainfall thresholds in excess of 2.54 mm (0.1 in) are shown.

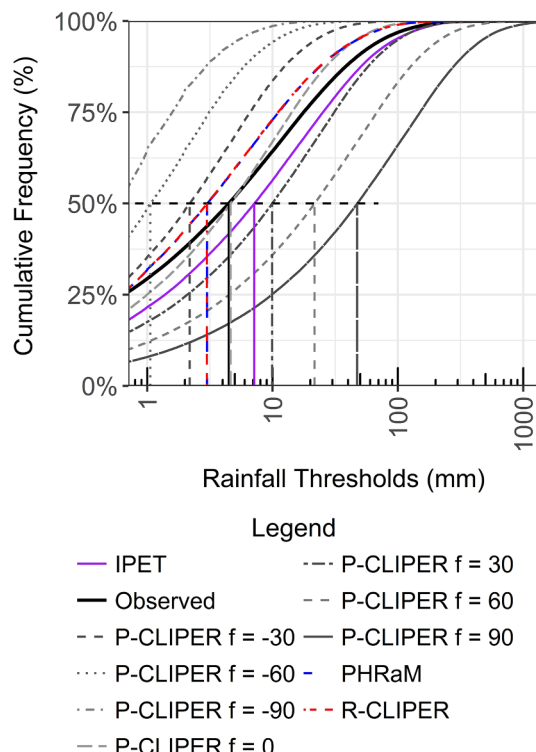


Fig. 9. Rainfall cumulative distribution functions (CDF) of rain flux within 500 km of the observed storm tracks for 2004–2017 Atlantic TCs producing rain over CONUS. The median value is shown with a dashed horizontal line.

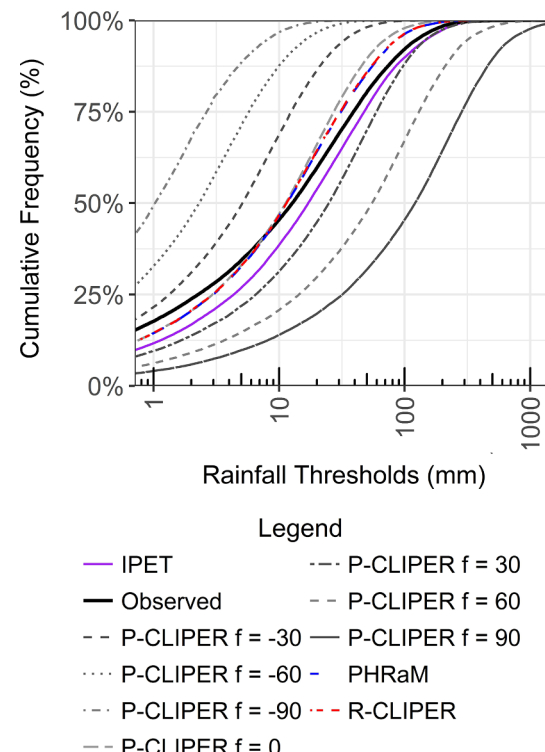


Fig. 11. CDF of rainfall within 100 km of the storm track for all models and observations of 2004–2017 Atlantic TCs producing rainfall over CONUS.

gradually return to under-predicting the higher rainfall amounts.

3.1.3. Extreme rain amounts

For analysis of TC rainfall-runoff flooding, it is also important to quantify how well each model predicts “extreme rain amounts”, defined

herein as those values in the top 5 percent of the observed CDF. The deviation of the model CDF curves from the observed CDF was quantified based on the large-scale CDF curves (the entire portion of the domain within 500 km of each storm track) and on the track-relative CDFs (over 100-km bands). A large-scale CDF curve depicting the 95th percentile storm-total rainfall of each model is shown in Fig. 12.

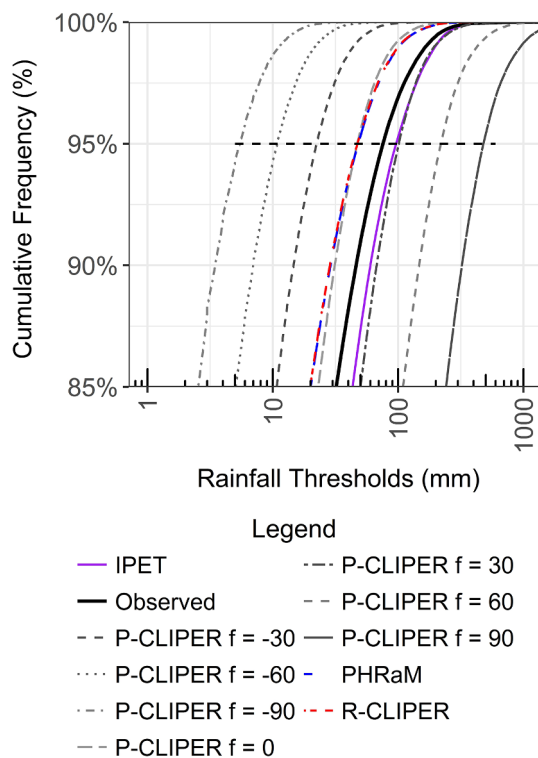


Fig. 12. CDF of rainfall at or above 85th percentile within 500 km of the storm track for all models and observations of 2004–2017 Atlantic TCs producing rainfall over CONUS.

For the storms in this study, the observed 95th percentile occurred at 75.7 mm (3 in). Each of the P-CLIPER variants with $f \leq -30$ did not produce any storm-total rainfall above 75.7 mm (3 in.), which is unsurprising since Geoghegan et al. (2018) found best-fit f -values ranging from -19 to $+50$ for 12 TCs from 2002 through 2008. Conversely, for $f \geq 60$, a much larger percentage of the model rainfall was above the observed 95th percentile; the maximum parameter value tested of $f = 90$ led to only 34.9% of model rainfall being less than or equal to 75.7 mm, meaning that 65.1% of P-CLIPER simulated values were above the 95th percentile of the observed data. PHRaM and R-CLIPER in general under-predicted storm-total rainfall, since the 75.7 mm threshold corresponded to 98.9% and 99.0% values on the CDF, respectively. The IPET model predicted 92.4% of storm-total values at or less than the 95th percentile of the observed, the closest fit by any model evaluated while still over-predicting the higher rainfall amounts. These CDF percentages over both large-scale and track-relative were translated into index values using the formulae set forth in M7. It is important to note that if a CDF did not contain the 95th percentile of the observed data at all, the skill for that band was set to zero.

3.1.4. Combined indices

A summary table of the various indices from each component of the analysis is presented in Table 7. While large-scale ETS values were fairly poor for all models on the 0.1-degree resolution grid, IPET and P-CLIPER with $f = 30$ performed the best. These ETS values improve substantially when interpolated to the HUC10 units as noted above. For the mean rainfall error index, IPET, PHRaM, R-CLIPER and P-CLIPER ($f = 0$) are roughly tied. IPET appears to be superior when measured by each of the CDF indices, whether median or 95th percentile, implying that IPET produces the most similar CDF curve of the models evaluated.

A combined index was calculated for each of the components evaluated in this study: pattern matching, mean/median/volume measures, and extreme rain amounts. The index for pattern matching was found by taking the arithmetic average of the mean correlation

over all storms and the rain flux-weighted ETS. The mean/median/volume measures were combined into a single index by taking the arithmetic average of the mean rainfall error index, the large-scale CDF median value index, and the track-relative CDF median value index. The index for extreme rain amounts was found by averaging the large-scale CDF maximum index with the track-relative CDF maximum index. The combined indices are presented in Table 8.

IPET outperforms PHRaM and R-CLIPER on all combined metrics, and IPET outperforms all variants of P-CLIPER tested in this study on all metrics except pattern matching.

3.2. 2017 Hurricane Harvey

Following the devastation in Harris County, Texas and surrounding areas due to the massive rainfall during 2017 Hurricane Harvey, a common question is whether proposed models will be sufficient to predict events such as Harvey prior to their occurrence. As done for the other simulated storms, simulations of TC rainfall were completed for the time period from 1200 UTC Aug 25, 2017 through 1200 UTC Sep 02, 2017 (for reference, Harvey made its first Texas landfall at its maximum strength of 115 kts at 0300 UTC Aug 26, 2017, per Blake and Zelinsky, 2018). Even with the meandering track Harvey followed, the maximum values of rainfall produced in each model were significantly less than observed in most cases. For instance, compared with the observed maximum value of 1539 mm over 5 days, IPET produced only as much as 479 mm, and PHRaM produced even less with a maximum of 441 mm. While P-CLIPER with $f = +60$ was able to match the observed amount well (1459 mm, about 95% of observed), it places the maximum rainfall over Corpus Christi, some 320 km southwest of the observed peak near Houston. On the other hand, while P-CLIPER with $f = +90$ (the maximum possible) is capable of producing almost exactly the right amount of precipitation over Houston (1550 mm compared with 1539 mm, an insignificant error at amounts that high and therefore uncertain), the scenario of $f = +90$ dramatically oversaturates the rest of the eastern Texas coast. The new value of the maximum rainfall is still over Corpus Christi with $f = +90$ since the placement of rain does not change with a change in f -value, but the value becomes 3071 mm, nearly double the observed peak over Houston. This indicates that while P-CLIPER is capable of producing the raw point maxima of rainfall occurring in Harvey (and much more), it may have issues placing it in the correct location, likely due to lack of physics that influenced Harvey's stall and therefore its rain structure. This should serve to indicate some of the potential failings of using climatological means (even if modified by various factors) since the governing physics is largely left out of calculations.

4. Conclusions and future work

Overall, when evaluated over the 2004–2017 Atlantic TCs, the IPET model currently demonstrates the highest skill for reproducing TC rainfall patterns based on the combination of the measures described herein, particularly because it conservatively over-predicts storm-total rainfall in most cases (i.e. those with less than 508 mm [20 in.] storm-total rainfall). However, it is important to realize that all statistical models presented in this study do not perform as well as the dynamical models in M7, nor even the statistical R-CLIPER used in M7. The lack of skill in using the statistical models in this study for 2004–2017 is to be expected since the statistical PHRaM, P-CLIPER, R-CLIPER and IPET models were all derived based on climatological mean rain rates from TRMM data measured in Lonfat et al. (2004) spanning TCs from only 1998–2002. Therefore, these statistical models were expected to demonstrate higher predictive skill for the time period used in M7 which includes their training data, 1998–2004, than for the completely unseen time period used in this study, 2004–2017. This effect would be enhanced further under climate change considerations which increase storm-total rainfall overall, based mainly on projected increases in

Table 7

Summary of Calculated Index Values. Boldface indicates the model with the best performance in each metric. P-CLIPER is evaluated separately from the other models.

	IPET	PHRaM		R-CLIPER			
	0.12	0.08	0.53	0.08			
Large-scale ETS	0.12	0.08	0.53	0.08			
Pattern Correlation	0.47	0.41	0.43	0.42			
Mean rainfall error index	0.52	0.53	0.52	0.52			
Large-scale CDF median value index	0.90	0.40	0.40	0.40			
Track-relative CDF median value index	0.81	0.32	0.32	0.31			
Large-scale CDF percentage in 95th percentile index	0.93	0.84	0.84	0.84			
Track-relative CDF percentage in 95th percentile	0.91	0.83	0.83	0.83			
	<u>P-CLIPER</u>						
	f = -90	f = -60	f = -30	f = 0	f = 30	f = 60	f = 90
Large-scale ETS	0.06	0.07	0.09	0.13	0.16	0.11	0.05
Pattern Correlation	0.38	0.40	0.42	0.43	0.43	0.43	0.43
Mean rainfall error index	0.05	0.11	0.24	0.52	0.46	0.00	0.00
Large-scale CDF median value index	0.12	0.20	0.36	0.79	0.31	0.00	0.00
Track-relative CDF median value index	0.15	0.16	0.20	0.46	0.45	0.22	0.00
Large-scale CDF percentage in 95th percentile index	0.00	0.00	0.00	0.85	0.84	0.00	0.00
Track-relative CDF percentage in 95th percentile	0	0	0.38	0.61	0.91	0.28	0.12

Table 8

Summary of Combined Index Values. Boldface indicates the model with the best performance in each metric. P-CLIPER is evaluated separately from the other models.

	IPET	PHRaM		R-CLIPER			
	0.26	0.23	0.42	0.84	0.23		
Pattern Matching	0.26	0.23	0.42	0.84	0.23		
Mean/Median/Volume	0.74	0.42	0.41	0.84	0.41		
Extreme Rain	0.92	0.84	0.84	0.84	0.84		
	<u>P-CLIPER</u>						
	f = -90	f = -60	f = -30	f = 0	f = 30	f = 60	f = 90
Pattern Matching	0.22	0.24	0.26	0.28	0.30	0.27	0.24
Mean/Median/Volume	0.11	0.16	0.27	0.59	0.41	0.07	0.00
Extreme Rain	0	0	0.19	0.73	0.88	0.14	0.06

rainfall intensity at large radii in landfalling storms, further increasing flood risk in large watersheds (Wright et al., 2015). As a result, the statistical models presented in this study need to be updated using more recent rainfall rate data with longer periods of record which are now available, as well as take into account uncertainty due to climate change effects. In their current state, none of the models is recommended for direct use in coastal flood studies. Once the statistical models (or other types of models, such as those derived using artificial neural networks or other supervised machine learning techniques, e.g. Bass and Bedient, 2018) are updated or created based on the most recent TC rainfall data, an engineering analysis of rainfall rates resulting from TCs can be undertaken.

The weakness of the current statistical models is underscored by the fact that for TCs producing massive amounts of precipitation such as 2017 Hurricane Harvey, only P-CLIPER with a substantially above-average frequency f value is capable of reproducing the large storm-total precipitation amounts. Regardless, care must be taken not to overfit f values, since tuning f large enough to reproduce one large peak observation may dramatically increase the total rain flux over a small (or large) area, seriously overestimating the expected flooding from rainfall-runoff.

Improvements from using the modified (no-shear) PHRaM over R-CLIPER are marginal at best for the 2004–2017 TC climatology as a whole. While this study attempted to consider statistical models which used only the five parameters typically used in JPM-OS, the addition of wind shear plays an important role in PHRaM's skill for the 2004–2017 Atlantic TCs, and future studies using the PHRaM model should include wind shear as an additional parameter in their JPM integral.

Furthermore, updated ETS statistics will be calculated as data become available from the 2018 TC season; 2018 Hurricanes Florence and Michael will be of particular interest. A similar methodology to the study presented herein is also proposed for evaluation of TC rainfall in Puerto Rico given its unique exposure and aggravating factor of mountainous slopes in comparatively smaller watersheds than present in CONUS. The model selection criteria established in this study will also be used to attempt to include rainfall-runoff forcing in future coastal flood risk studies.

Declaration of Competing Interest

The authors declare that they have no known competing financial interests or personal relationships that could have appeared to influence the work reported in this paper.

Acknowledgements

The first author was financially supported by the Center for the Management, Utilization and Protection of Water Resources at Tennessee Technological University (TTU). The authors are grateful to Timothy Marchok and Robert Tuleya of the National Oceanic and Atmospheric Administration's Geophysical Fluid Dynamics Laboratory (NOAA GFDL) for assistance with use of their skill indices. Additionally, the authors would like to thank three anonymous reviewers for their suggestions which improved the manuscript.

References

- Bacopoulos, P., Tang, Y., Wang, D., Hagen, S.C., 2017. Integrated hydrologic-hydrodynamic modeling of estuarine-riverine flooding: 2008 Tropical Storm Fay. *J. Hydrol. Eng.* 22 (8). [https://doi.org/10.1061/\(ASCE\)HE.1943-5584.0001539](https://doi.org/10.1061/(ASCE)HE.1943-5584.0001539).
- Bass, B., Bedient, P., 2018. Surrogate modeling of joint flood risk across coastal watersheds. *J. Hydrol.* 558, 159–173. <https://doi.org/10.1016/j.jhydrol.2018.01.014>.
- Blake, E.S., Zelinsky, D.A., 2018. National Hurricane Center Tropical Cyclone Report: Hurricane Harvey (AL092017). National Hurricane Center (NHC), Miami, FL.
- Bunya, S., Dietrich, J.C., Westerink, J.J., Ebersole, B.A., Smith, J.M., Atkinson, J.H., Jensen, R., Resio, D.T., Luettich, R.A., Dawson, C., Cardone, V.J., Cox, A.T., Powell, M.D., Westerink, H.J., Roberts, H.J., 2010. A high-resolution coupled riverine flow, tide, wind, wind wave and storm surge model for southern Louisiana and Mississippi: part I—model development and validation. *Mon. Weather Rev.* 138 (2), 345–377. <https://doi.org/10.1175/2009MWR2906.1>.
- Cangialosi, J.P., Latto, A.S., Berg, R., 2018. National Hurricane Center Tropical Cyclone Report: Hurricane Irma (AL112017). National Hurricane Center (NHC), Miami, FL.
- Chen, S.S., Knaff, J.A., Marks, F.D., 2006. Effects of vertical wind shear and storm motion on tropical cyclone rainfall asymmetries deduced from TRMM. *Mon. Weather Rev.* 134 (11), 3190–3208. <https://doi.org/10.1175/MWR3245.1>.
- Crossett, K., Ache, B., Pacheco, P., Haber, K., 2013. NOAA State of the Coast National Coastal Population Report: Population Trends from 1970 to 2020. National Oceanic and Atmospheric Administration, Silver Spring, MD.
- Demuth, J., DeMaria, M., Knaff, J.A., 2006. Improvement of advanced microwave sounder unit tropical cyclone intensity and size estimation algorithms. *J. Appl. Meteor.* 45, 1573–1581. <https://doi.org/10.1175/JAM2429.1>.
- Dietrich, J.C., Bunya, S., Westerink, J.J., Ebersole, B.A., Smith, J.M., Atkinson, J.H., Jensen, R., Resio, D.T., Luettich, R.A., Dawson, C., Cardone, V.J., Cox, A.T., Powell, M.D., Westerink, H.J., Roberts, H.J., 2010. A high-resolution coupled riverine flow, tide, wind, wind wave and storm surge model for southern Louisiana and Mississippi: part II—Synoptic Description and Analysis of Hurricanes Katrina and Rita. *Mon. Weather Rev.* 138 (2), 378–404. <https://doi.org/10.1175/2009MWR2907.1>.
- Divoky, D., Resio, D.T., 2007. Performance of the JPM and EST methods in storm surge studies. *Proc., 10th International Workshop on Wave Hindcasting and Forecasting and Coastal Hazard Symposium*. Joint WMO/IOC Technical Commission for Oceanography and Marine Meteorology. Oahu, Hawaii, USA.
- Fleming, J., Fulcher, C., Luettich Jr., R.A., Estrade, B., Allen, G., Winer, H., 2008. A real time storm surge forecasting system using ADCIRC. In: Spaulding, M.L. (Ed.), *Proc., Estuarine and Coastal Modeling X*. ASCE, pp. 373–392.
- Generalized Bathymetric Chart of the Oceans (GEBCO), 2015, version 20150318, www.gebco.net.
- Geoghegan, K.M., Fitzpatrick, P., Kolar, R.L., Dresback, K.M., 2018. Evaluation of a synthetic rainfall model, P-CLIPER, for use in coastal flood modeling. *Nat. Hazards* 92 (2), 699–726. <https://doi.org/10.1007/s11069-018-3220-4>.
- Grieser, J., Jewson, S., 2012. The RMS TC-rain model. *Meteorologische Zeitschrift* 21 (1), 79–88. <https://doi.org/10.1127/0941-2948/2012/0265>.
- Holland, G.J., 1980. An analytic model of the wind and pressure profiles in hurricanes. *Mon. Weather Rev.* 108 (8), 1212–1218. [https://doi.org/10.1175/1520-0493\(1980\)108<1212:AAMOTW>2.0.CO;2](https://doi.org/10.1175/1520-0493(1980)108<1212:AAMOTW>2.0.CO;2).
- Interagency Performance Evaluation Task Force (IPET), 2006. “Performance evaluation of the New Orleans and Southeast Louisiana Hurricane Protection System draft final report of the Interagency Performance Evaluation Task Force volume VIII – engineering and operational risk and reliability analysis”.
- Knabb, R.D., Rhome, J.R., Brown, D.P., 2005. Tropical Cyclone Report: Hurricane Katrina. National Hurricane Center (NHC), Miami, FL.
- Langousis, A., Veneziano, D., 2009. Theoretical model of rainfall in tropical cyclones for the assessment of long-term risk. *J. Geophys. Res.* 114 (D2). <https://doi.org/10.1029/2008JD010080>.
- Lin, Y., 2011. GCIP/EOP Surface: Precipitation NCEP/EMC 4KM Gridded Data (GRIB) Stage IV Data. Version 1.0. UCAR/NCAR - Earth Observing Laboratory. DOI:10.5065/D6PG1QDD. (accessed 02 Oct 2018).
- Lonfat, M., Marks, F.D., Chen, S.S., 2004. Precipitation distribution in tropical cyclones using the Tropical Rainfall Measuring Mission (TRMM) microwave imager: a global perspective. *Mon. Weather Rev.* 132 (7), 1645–1660. [https://doi.org/10.1175/1520-0493\(2004\)132<1645:PDITCU>2.0.CO;2](https://doi.org/10.1175/1520-0493(2004)132<1645:PDITCU>2.0.CO;2).
- Lonfat, M., Rogers, R., Marchok, T., Marks Jr., F.D., 2007. A parametric model for predicting hurricane rainfall. *Mon. Weather Rev.* 135 (9), 3086–3097. <https://doi.org/10.1175/MWR3433.1>.
- Luettich, R.A., Westerink, J.J., 2004. “Formulation and numerical implementation of the 2D/3D ADCIRC finite element model version 44.XX” Available from: https://adcirc.org/files/2018/11/adcirc_theory_2004_12_08.pdf.
- Marchok, T., Rogers, R., Tuleya, R., 2007. Validation schemes for tropical cyclone quantitative precipitation forecasts: evaluation of operational models for U.S. landfalling cases. *Weather Forecasting* 4, 726–746. <https://doi.org/10.1175/WAF1024.1>.
- Marks, F.D., DeMaria, M., 2003. “Development of a tropical cyclone rainfall climatology and persistence (R-CLIPER) model”. Technical report, NOAA/OAR/AOML/Hurricane Research Division.
- Myers, V.A., 1975. “Storm tide frequencies on the South Carolina coast”. NOAA Technical Report NWS-16.
- Orton, P., Georgas, N., Blumberg, A., Pullen, J., 2012. Detailed modeling of recent severe storm tides in estuaries of the New York City region. *J. Geophys. Res.* 117, C09030. <https://doi.org/10.1029/2012JC008220>.
- Orton, P., Conticello, F., Cioffi, F., Hall, T., Georgas, N., Lall, U., Blumberg, A., 2015. Hazard assessment from storm tides and rainfall on a tidal river estuary. *Proc., 16th International Association for Hydro-Environment Engineering and Research (IAHR) World Congress*. 28 Jun.-3 Jul. 2015; The Hague; Netherlands. Report Number GSFC-E-DAA-TN24935.
- Orton, P., Conticello, F., Cioffi, F., Hall, T., Georgas, N., Lall, U., Blumberg, A., MacManus, K., 2018. Flood hazard assessment from storm tides, rain and sea level rise for a tidal river estuary. *Nat. Hazards* 2018, 1–29. <https://doi.org/10.1007/s11069-018-3251-x>.
- Ray, T., Stepiniski, E., Sebastian, A., Bedient, P.B., 2011. Dynamic modeling of storm surge and inland flooding in a Texas coastal floodplain. *J. Hydraul. Eng.* 137 (10), 1103–1110. [https://doi.org/10.1061/\(ASCE\)HY.1943-7900.0000398](https://doi.org/10.1061/(ASCE)HY.1943-7900.0000398).
- Reed, S.M., Maidment, D.R., 1999. Coordinate transformations for using NEXRAD data in GIS-based hydrologic modeling. *J. Hydrol. Eng.* 4 (2), 174–182. [https://doi.org/10.1061/\(ASCE\)1084-0699\(1999\)4:2\(174\)](https://doi.org/10.1061/(ASCE)1084-0699(1999)4:2(174)).
- Resio, D.T., 2007. White Paper on Estimating Hurricane Inundation Probabilities. Available from, Engineering Research and Development Center, Coastal and Hydraulics Laboratory, Vicksburg, MS. <http://hdl.handle.net/11681/22643>.
- Scheffner, N.W., Clausner, J.E., Militello, A., Borgman, L.E., Edge, B.L., Grace, P.J., 1999. “Use and application of the Empirical Simulation Technique: User’s Guide”. U.S. Army Engineer Research and Development Center, Vicksburg, Mississippi, Technical Report CHL-99-21.
- Toro, G.R., Niedoroda, A.W., Reed, C., Divoky, D., 2010. Quadrature-based approach for the efficient evaluation of surge hazard. *Ocean Eng.* 37 (1), 114–124. <https://doi.org/10.1016/j.oceaneng.2009.09.005>.
- Torres, J.M., Bass, B., Irza, N., Fang, Z., Proft, J., Dawson, C., Kiani, M., Bedient, P., 2015. Characterizing the hydraulic interactions of hurricane storm surge and rainfall-runoff for the Houston-Galveston region. *Coast Eng.* 106, 7–19. <https://doi.org/10.1016/j.coastaleng.2015.09.004>.
- Tuleya, R.E., DeMaria, M., Kuligowski, R.J., 2007. Evaluation of GFDL and simple statistical model rainfall forecasts for U.S. landfalling tropical storms. *Weather Forecasting* 22 (1), 56–70. <https://doi.org/10.1175/WAF972.1>.
- Wright, D.B., Knutson, T.R., Smith, J.A., 2015. Regional climate model projections of rainfall from U.S. landfalling tropical cyclones. *Clim. Dyn.* 45, 3365–3379. <https://doi.org/10.1007/s00382-015-2544-y>.